

Article

Comprehensive Modeling and Safety Protection Strategy for Thermal Runway Propagation in Lithium-Ion Battery Modules under Multi-Factor Influences

Zhixiong Chai ¹, Junqiu Li ^{1,*}, Ziming Liu ¹, Zhengnan Liu ¹ and Xin Jin ²

¹ National Engineering Research Center of Electric Vehicles, Beijing Institute of Technology, Beijing 100081, China; 3120195246@bit.edu.cn (Z.C.); 3120205223@bit.edu.cn (Z.L.); bit_lzn@163.com (Z.L.)

² Beijing Institute of Space Launch Technology, Beijing 100076, China; jx493067818@126.com

* Correspondence: lijunqiu@bit.edu.cn; Tel.: +86-136-2123-9752

Abstract: This paper addresses the challenge of thermal runaway propagation in lithium-ion battery modules and presents a safety protection design method based on a thermal propagation model. Firstly, it systematically analyzes the triggering mechanisms of thermal runaway in batteries, establishes a model for cell thermal runaway, and calibrates the model parameters through experiments. Secondly, by integrating the cell thermal runaway model and considering the three-dimensional structure of the battery module, a comprehensive thermal runaway propagation model is developed and validated. Subsequently, a simulation study on thermal runaway propagation, incorporating multi-factor influences and typical operating conditions, is conducted using the established thermal propagation model for the battery module. The study elucidates the thermal runaway propagation characteristics of the battery module under different safety protection strategies. The findings highlight that the proposed safety protection strategy effectively mitigates thermal propagation within the battery module, particularly when the thermal runaway is influenced by multiple factors.



Citation: Chai, Z.; Li, J.; Liu, Z.; Liu, Z.; Jin, X. Comprehensive Modeling and Safety Protection Strategy for Thermal Runway Propagation in Lithium-Ion Battery Modules under Multi-Factor Influences. *Batteries* **2024**, *10*, 31. <https://doi.org/10.3390/batteries10010031>

Academic Editor: Carlos Ziebert

Received: 12 December 2023

Revised: 15 January 2024

Accepted: 16 January 2024

Published: 18 January 2024



Copyright: © 2024 by the authors. Licensee MDPI, Basel, Switzerland. This article is an open access article distributed under the terms and conditions of the Creative Commons Attribution (CC BY) license (<https://creativecommons.org/licenses/by/4.0/>).

1. Introduction

Lithium-ion batteries are widely used in new energy vehicles due to their high energy density, long cycle life, high operating voltage, low memory effect, and other advantages. Due to the strong policy support for the new energy vehicle industry, it is developing rapidly, so lithium-ion batteries are also widely used in the market. However, in recent years, accidents involving lithium-ion battery fires and explosions have occurred occasionally, and the safety of lithium-ion batteries has become the focus of the public, industry, and researchers [1]. Hence, investigating lithium-ion batteries' Thermal Runaway Propagation (TRP) behavior holds considerable practical significance. Moreover, proposing an appropriate design scheme for protecting battery modules is imperative in this context.

Currently, the causes of the thermal runaway of batteries are categorized into electrical abuse, thermal abuse, and mechanical abuse [1], including overcharge abuse, external short-circuit abuse, high-temperature abuse, needle penetration abuse, and extrusion abuse. The mechanism of battery thermal runaway is a chain reaction when the temperature of the battery rises abnormally; it will trigger side reactions such as the solid electrolyte interface (SEI) film decomposition, the negative electrode and electrolyte reaction, etc., and the side reactions will release a large amount of heat to promote the side reactions further, forming a chain reaction [2]. Ren et al. used differential scanning calorimetry to analyze the reaction kinetics of the main side reactions of the battery in a quantitative manner. They established a thermal runaway model that can accurately predict the thermal runaway behavior under high-temperature abuse based on the Arrhenius formula [3]. For the lithium-ion phosphate

system, Bugryniec et al. also carried out a large number of studies on thermal runaway, including 18,650 batteries [4] and square aluminum shell batteries [5], and the reaction kinetic parameters of the same system are almost the same.

Considering that current automotive lithium-ion batteries are used in large-scale modules, there is a risk of TRP to the battery module once thermal runaway occurs in a cell [6]. Researchers have carried out experimental and modeling studies on the TRP of different battery systems, and the experimental and simulation results show that, in most battery modules, the thermal runaway of a cell will propagate to the whole module [7,8]. For the evaluation criteria of the TRP of batteries, most studies consider the thermal runaway trigger temperature as the standard (the national standard is 1 °C/s, and it lasts for more than 3 s [9]). Once a battery experiences a valve leakage, a substantial accumulation of combustible gas and electrolytes occurs within the battery casing, escalating the risk of TRP [10]. Therefore, by advancing the evaluation criterion for TRP from the thermal runaway triggering temperature to the temperature of battery valve leakage, it is possible further to enhance the safety of thermal protection in batteries.

Studies have shown that the heat transfer, electrical connection, and thermal runaway ejection of combustible objects are the main factors triggering TRP. The TRP behavior caused by the high temperature of the battery is mainly analyzed from the perspective of heat conduction. Weng [11] et al. showed that aerogel has an excellent performance in regard to slowing down the propagation of the thermal runaway of batteries. At the same time, the aerogel's density is similar to that of air, which will not increase the weight of the battery system, and it is an ideal flame-retardant protective material. However, the above studies on battery TRP and safety protection only focus on the protection effect of battery modules under a single or typical working condition of thermal propagation.

This paper focuses on the thermal runaway propagation issues in lithium iron phosphate (LiFePO₄) batteries. Through establishing a TRP model for batteries, this study investigates the TRP behavior of battery modules under typical operating conditions and the influence of multiple factors, aiming to achieve the safety protection design of battery modules. Initially, the analysis and categorization of triggering mechanisms for the cell thermal runaway are conducted, with experimental data employed to calibrate the model. Subsequently, a TRP model for the battery module is established, and experimental validation is carried out. Ultimately, safety protection simulations for battery modules are conducted, involving the simulation analysis of the TRP boundaries and safety protection design boundaries under the influence of multiple factors. Simulation validation is performed explicitly for typical operating conditions.

2. Material and Method

2.1. Battery Basic Parameters

This paper uses a 32 Ah lithium iron phosphate square aluminum case battery as a research object. The battery is sourced from EVE Energy Co., Ltd. in Huizhou City, Guangdong Province, China. Table 1 gives the basic parameters of this battery.

Table 1. Specifications of the 32 Ah LiFePO₄ battery.

Specifications	Values
Rated capacity	32 Ah
Rated voltage	3.2 V
Cutoff voltage range	2.5 V~3.65 V
Geometry	148 mm × 91.5 mm × 26.7 mm
Mass	725 ± 50 g
Cell type	Prismatic cell

The corresponding thermophysical parameters of the battery are as follows (Table 2). The battery's density and specific heat capacity are the actual measured parameters, and

the thermal conductivity refers to the parameters of the same square-shell LiFePO₄ system in the literature [5].

Table 2. Thermophysical parameters of the battery.

Parameters	Notation	Numerical Value	Unit
Intensity ^a	ρ	4094.4	kg/m ³
Thermal capacity ^a	c_p	1017	J/(kg·K)
	k_x	0.8348	W/(K·m)
Thermal conductivity [5]	k_y	18.034	W/(K·m)
	k_z	18.034	W/(K·m)
Convective heat transfer coefficient ^b	h	7.5	W/(K·m ²)

^a Experimental measurement; ^b estimation based on empirical values.

2.2. Heat Transfer Theory

Cell heat conduction adheres to Fourier's law of thermal conductivity, and the three-dimensional heat conduction equation is expressed as

$$C_p M \frac{\partial T}{\partial t} = \frac{\partial}{\partial x} \left(k_x \frac{\partial T}{\partial x} \right) + \frac{\partial}{\partial y} \left(k_y \frac{\partial T}{\partial y} \right) + \frac{\partial}{\partial z} \left(k_z \frac{\partial T}{\partial z} \right) + Q_t - Q_p \quad (1)$$

where M is the battery mass, C_p is the constant pressure heat capacity of the battery, k is the thermal conductivity of the battery, Q_t is the additional heat input, and Q_p is the ambient heat dissipation.

The heat dissipation of lithium batteries in the environment is currently accounted for solely through convection, neglecting surface heat conduction and radiation. The convective heat exchange between the battery and the external environment is governed by Newton's law of cooling:

$$Q = Ah(T_s - T_{amb}) \quad (2)$$

where A is the convective heat transfer area of the battery, h is the convective heat transfer coefficient, T_s is the temperature of the battery surface, and T_{amb} is the ambient temperature.

2.3. Battery Thermal Runaway Modeling Method

(1) Modeling of side-effect mechanisms

The battery temperature continues rising and triggers the self-exothermic side reactions, accelerating the evolution of the thermal runaway. This paper mainly considers the four main side reactions: the SEI film decomposition reaction, the negative electrode decomposition reaction, the positive electrode decomposition reaction, and the electrolyte oxidation reaction. Moreover, the exothermic rate of each reaction is described according to Arrhenius' formula. The cumulative heat generation rates induced by the side reactions are computed using the following equation:

$$Q_{\text{side}} = Q_{\text{sei}} + Q_{\text{ne}} + Q_{\text{pe}} + Q_e \quad (3)$$

where Q_{sei} , Q_{ne} , Q_{pe} and Q_e correspond to the heat generation rate per unit volume of the four side reactions mentioned above, in W/m⁻³.

SEI film is formed during the first cycle of the battery to avoid the negative electrode directly reacting with the electrolyte, and it is easy to decompose and exothermic at 80~120 °C [12]. The following equation can describe the decomposition reaction process and its heat generation rate:

$$\begin{cases} \frac{dc_x}{dt} = -A_x \exp\left(-\frac{E_{a,x}}{RT}\right) f_x(c_x) g_x \\ Q_x = -H_x W_x \frac{dc_x}{dt} \end{cases} \quad (4)$$

where x can represent sei (SEI film), ne (negative reaction), pe (positive reaction), and e (electrolyte reaction); T is the temperature of the cell in K; c_x is a dimensionless quantity, which represents the concentration of the reactants; A_x , $E_{a,x}$, $f_x(c_x)$, and g_x represent the frequency factor, the activation energy of the reaction, the relationship between the reaction rate and the concentration of the reactants, and the correction term of the reaction, respectively; H_x denotes the exothermic heat of the reaction per unit of weight in J/kg; W_x is the mass per unit volume of reactants in kg/m³; and R is the ideal gas constant.

Then, the electrolyte reacts with the negative electrode when the temperature reaches around 120 °C, generating heat of Q_{ne} [13]. Then, the positive electrode decomposes partially at around 160 °C with the heat of Q_{pe} [14]. The electrolyte can decompose exothermically at elevated temperatures (>200 °C), as Q_e [15].

(2) Thermal runaway trigger modeling

The thermal runaway side-reaction heat generation described above occurs significantly only when the battery temperature surpasses 80~100 °C. Consequently, it becomes imperative to model the catalytic heat, $Q_{trigger}$, associated with thermal runaway before the temperature rises from ambient conditions to initiate the side reaction.

The thermal runaway of batteries can be classified into three types of misuse based on their triggering mechanisms: mechanical abuse (e.g., needle penetration and compression), electrical abuse (including overcharge, internal short circuit, and external short circuit), and thermal abuse (such as exposure to high temperatures). These triggering mechanisms are interconnected and can influence one another. For instance, in the case of mechanical abuse, deformation of the battery may result in the rupture of internal separators. This deformation can lead to contact between positive and negative electrodes, causing an internal short circuit and electrical abuse. The progression of an internal short-circuit generates abnormal heat, leading to a rapid temperature rise and eventual thermal abuse. The heightened temperature induced by various forms of misuse can ultimately trigger thermal runaway.

In the context of TRP within a battery module, cells undergoing thermal runaway generate a significant amount of abnormal heat. This abnormal heat is predominantly transferred to adjacent cells through thermal conduction, heating normal cells and subsequently triggering thermal runaway. In this study, the analysis of battery thermal propagation behavior categorizes triggering events leading to thermal runaway into two modes based on the abnormal heat generation rate of cells in thermal runaway: the slow heat-generation mode associated with fault evolution and the rapid heat-generation mode associated with sudden abuse.

a. Fault evolution thermal runaway-trigger modeling method

The abnormal heat production rate of the battery module is comparatively low, leading to a gradual initiation of battery thermal runaway, characterized by an extended duration. The thermal runaway is instigated by heat sources, encompassing internal chemical reactions within the battery and the heat generated during the charging and discharging cycles.

$$Q_{trigger} = f(T) + Q_{normal} \quad (5)$$

where $f(T)$ is the chemical reaction heat generation in the fault evolution, which is related to the battery temperature and fitted via the experiment; and Q_{normal} is the heat generation in the charging and discharging cycle.

Take overcharge abuse as an example. The chemical reaction occurring within the battery is the reaction between plated lithium and electrolyte induced by overcharging. The rate of reaction can be mathematically expressed as follows (6) [16]. The reaction rate is represented by the following:

$$\frac{dn_{Li}}{dt} = A_{Li} \cdot \exp\left(-\frac{E_{a,Li}}{RT}\right) \cdot \frac{k_{Li} \cdot n_{Li}}{1+k_{Li}n_{Li}} \cdot c_e \\ f(T) = -H_{Li}W_{Li} \frac{dn_{Li}}{dt} \quad (6)$$

where n_{Li} is the amount of the deposited lithium on the anode, A_{Li} is the frequency factor of the reaction, $E_{a,Li}$ is the activation energy of the reaction, H_{Li} is the reaction heat per unit mass of lithium plating, W_{Li} is the reaction mass of lithium plating, and $\frac{k_{Li} \cdot n_{Li}}{1+k_{Li}n_{Li}}$ determines whether or not the reaction occurs between lithium and electrolyte. When $n_{Li} \gg 1$, $\frac{k_{Li} \cdot n_{Li}}{1+k_{Li}n_{Li}}$ is equal to 1, the reaction occurs; when $n_{Li} = 0$, $\frac{k_{Li} \cdot n_{Li}}{1+k_{Li}n_{Li}}$ is equal to 0, then the reaction does not occur [13].

Bernardi's heat generation rate equation can calculate the general case of heat production in charge/discharge cycles. Considering that the overcharge process is mainly battery ohmic heat generation, it can be simplified by (7):

$$Q_{normal} \approx Q_{ohm} = I_{load}^2 \cdot r(SOC) \quad (7)$$

where I_{load} is the charging current, and $r(SOC)$ is the DC internal resistance obtained experimentally.

b. Sudden abuse thermal runaway-trigger modeling method

In the case of thermal runaway triggered by sudden abuse, the battery module exhibits a relatively high abnormal heat production rate, resulting in a rapid initiation of battery thermal runaway. The time required for thermal runaway triggered by sudden abuse is short. The thermal runaway trigger in this context can be simplified as follows:

$$Q_{trigger} = f(t) \quad (8)$$

where $f(t)$ is the heat generation of sudden abuse, time-dependent, fitted by experiment.

Therefore, the total heat generated by the thermal runaway of the battery is as follows:

$$Q_{all} = Q_{side} + Q_{trigger} \quad (9)$$

where Q_{all} represents the total additional heat.

2.4. Experiment

In accordance with the aforementioned modeling requirements analysis and subsequent verification of the TRP model for the battery module, experiments were conducted as outlined in Table 3. Experiments 1, 2, and 3 were carried out to calibrate the parameters of the battery cell and acquire cell temperature data. Experiments 4 and 5 were executed to validate the TRP module model and gather temperature data for each cell within the battery module. A K-type thermocouple was affixed to the center of the battery, and the Fluke 2638A data acquisition instrument, sourced from Fluke Corporation (Everett, WA, USA), was employed to collect battery temperature data. The thermocouple measurement accuracy is 0.5 °C. Further details regarding the experiments are provided in the subsequent section.

Table 3. Battery thermal runaway and TRP experiment.

Number	Experimental Name	Experimental Subject	Data Acquisition	Experimental Objective
1	ARC experiment	LF32 cell	Cell temperature	Thermal runaway model parameter calibration
2	Cell needle penetration experiment	LF32 cell	Cell temperature	Fault evolution model parameter calibration
3	Cell overcharge experiment	LF32 cell	Cell temperature	Sudden abuse model parameter calibration
4	Module needle penetration experiment	LF32 module	Multiple cell temperature	TRP module model validation
5	Module overcharge experiment	LF32 module	Multiple cell temperature	TRP module model validation

3. Model Calibration and Validation

3.1. Cell Thermal Runaway Model Calibration

(1) Parameter calibration of the side-reaction mechanism model

The Accelerating Rate Calorimeter (ARC) experiment simulates the thermal characteristics of the exothermic reaction process within a battery, particularly when the internal heat cannot be dissipated on time, making the reaction more representative of actual conditions. Figure 1 depicts the temperature variations observed during the ARC experiment for a battery at 100% state of charge (SOC). At $T_1 = 97.66\text{ }^{\circ}\text{C}$, a temperature rise exceeding $0.02\text{ }^{\circ}\text{C}/\text{min}$ was recorded, prompting the cessation of heating and maintaining an adiabatic state. Subsequently, the battery's pressure relief valve opened at approximately $T_{\text{vent}} = 141.20\text{ }^{\circ}\text{C}$, and the temperature continued to escalate, reaching $T_2 = 197.35\text{ }^{\circ}\text{C}$ when the temperature rise rate surpassed $1\text{ }^{\circ}\text{C}/\text{s}$, indicative of a thermal runaway trigger. The temperature then continued to rise to its peak measurement point, $T_3 = 419.74\text{ }^{\circ}\text{C}$.

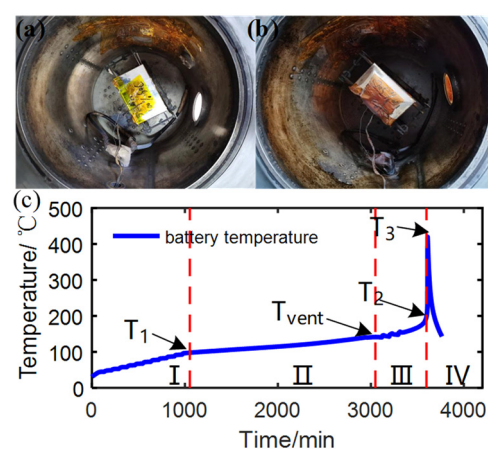


Figure 1. Battery ARC experiment: (a) pre-experiment photo, (b) post-experiment photo, and (c) battery temperature curve includes four stages of thermal runaway: I, II, III and IV.

Given that the battery may release substantial amounts of combustible gases and potentially splash a significant volume of electrolytes once entering Stage III, safety hazards such as external short circuits and combustible gas combustion exist. Consequently, for the safety assessment of battery thermal propagation, it is imperative to ensure that the battery temperature does not exceed the opening temperature of the pressure relief valve ($141.20\text{ }^{\circ}\text{C}$). Therefore, the temperature of the battery relief valve serves as the thermal propagation boundary.

Figure 2 presents the comparative results between simulation and experimentation for the model of the side-reaction mechanism. The goodness of fit of the simulated cell temperature to the experimental temperature is denoted as R^2 is 0.84473. The proximity of R^2 to 1 indicates the degree to which the model aligns with the experimental data and is calculated as follows:

$$R^2 = 1 - \sum_{i=1}^n (y_i - \hat{y}_i)^2 / \sum_{i=1}^n (y_i - \bar{y}_i)^2 \quad (10)$$

where n represents the number of samples, y_i represents the actual value of the i sample, \hat{y}_i represents the predicted value of the model for the i sample, and \bar{y}_i is the average value of all samples.

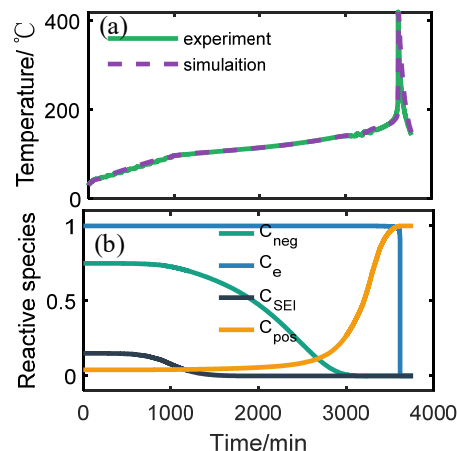


Figure 2. Battery side-reaction mechanism model. (a) Comparison of experimental and simulated temperature rise in the battery. (b) Simulated evolution of the dimensionless concentrations of the reactive species during the ARC test.

Table 4 lists the results of the calibration of the model parameters; g_x is the calibration result of the experimental cell, and the other parameters are the parameters obtained by comparing the cells of the same system in References [4,5,17].

Table 4. Parameters of lithium-ion battery side reaction.

Parameter Symbol	SEI Decomposition Reaction	Negative Electrode Reacts with Solvent	Positive Electrode Reacts with Solvent	Electrolyte Decomposition
$E_{a,x}$	1.38×10^5	1.32×10^5	0.99×10^5	2.70×10^5
A_x	1.66×10^{15}	2.5×10^{13}	2×10^8	5.14×10^{25}
$f_x(c_x)$	c_{sei}	c_{ne}	$c_{\text{pe}}(1 - c_{\text{pe}})$	c_e
g_x	1	1	1	2.3
$c_{x,0}$	0.15	0.75	0.04	1
H_x	2.57×10^5	1.714×10^5	1.947×10^5	6.2×10^5
W_x	1690	220	520.74	334.68

- (2) Calibration of the thermal runaway trigger model's parameters
 - a. Parameter calibration of the fault evolution model

To complete the calibration of the experimental parameters for the fault evolution trigger model, a single overcharge thermal runaway experiment was conducted at a 0.5 C multiplication rate (16 A). Charging was intermittently halted at 5% SOC intervals for 10 s during the overcharge stage to obtain the internal resistance of the battery [16], as illustrated in Figure 3. During the 0.5 C overcharge scenario, the single cell reached 116% SOC, and the CO gas sensor promptly detected the battery venting valve. Subsequently, overcharging persisted, leading to an accelerated rise in battery temperature. Thermal runaway was triggered at 125% SOC, accompanied by releasing a significant amount of white smoke. Although thermal runaway occurred, the maximum temperature reached was 300 °C, and no explosion or fire was observed in the lithium iron phosphate battery.

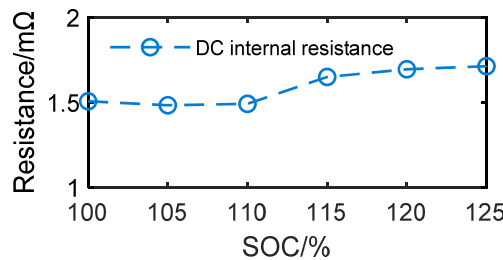


Figure 3. Battery internal resistance.

In consideration of the numerous lithium plating reaction parameters during overcharging, the catalytic heat is simplified into polynomial form, as indicated in Equation (11). The fitting results are depicted in Figure 4, and the corresponding parameters are presented in Table 5.

$$f(T) = \frac{p_1 T^3 + p_2 T^2 + p_3 T + p_4}{T^3 + q_1 T^2 + q_2 T + q_3} \quad (11)$$

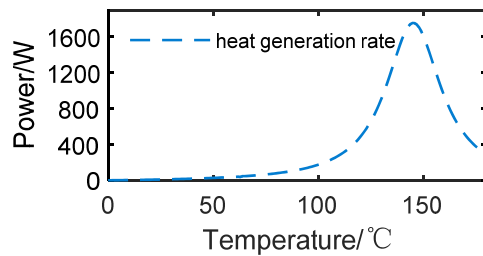


Figure 4. Heat generation rate of lithium-plating reaction.

Table 5. Fitting parameters for the heat generation rate of the lithium-plating reaction.

Parameters	Value	Parameters	Value
p_1	-20.01	q_1	-354
p_2	7184	q_2	3.978×10^4
p_3	-3.636×10^5	q_3	-1.353×10^6
p_4	-6.714×10^5		

Utilizing the thermal runaway side-reaction mechanism model and the fault evolution trigger model, the calibration of the thermal runaway model for cell fault evolution was successfully accomplished. The simulated battery temperature is compared with the corresponding experimental temperature in Figure 5. The goodness of fit (R^2) for the simulation data to the two sets of experimental temperature data is 0.99268 and 0.99859, respectively, demonstrating a high level of model accuracy.

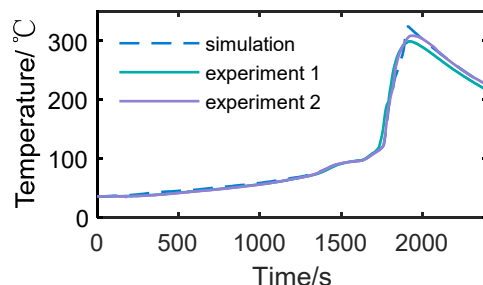


Figure 5. Comparison of thermal runaway simulation and experimental temperatures for fault evolution.

b. Parameter calibration of the sudden abuse trigger model

To finalize the calibration of the experimental parameters for the sudden abuse trigger model, we conducted a thermal runaway experiment on a cell battery, using needle penetration. A 5 mm diameter needle punctured the center of a 100% SOC battery at a depth of 20 mm (75% of the battery thickness). Following the puncture, the temperature escalated rapidly, and the battery's pressure relief valve opened, emitting a significant amount of smoke and triggering the thermal runaway of the battery. The temperature reached 300 °C within 100 s.

Utilizing the temperature-rise data from the battery, a Gaussian curve was fitted using Equation (12). The Gaussian curve was employed to fit the heat generation resulting from the sudden abusive contact of the battery, and all internally generated short-circuit heat was released within 100 s after the battery initiated an internal short circuit. The fitting results are displayed in Figure 6, with corresponding parameters presented in Table 6.

$$f(t) = a_1 \times \exp\left(-\frac{(t - b_1)^2}{c_1}\right) \quad (12)$$

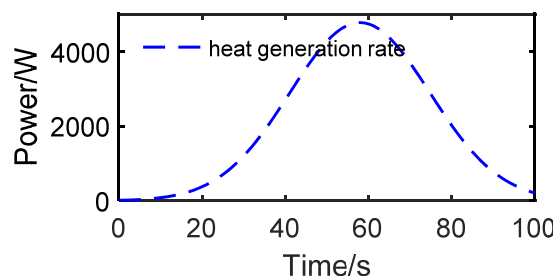


Figure 6. Heat generation rate of internal short circuit.

Table 6. Fitting parameters for heat generation rate of the internal short circuit.

Parameters	a_1	b_1	c_1
Parameter value	4776	57.93	57.93

With the completion of the thermal runaway side-reaction mechanism model and the sudden abuse trigger model, the calibration of the sudden abuse thermal runaway model is accomplished. The comparison between the simulated battery temperature and the experimental temperature is illustrated in Figure 7. The goodness of fit (R^2) for the simulation data to experimental temperature data is 0.99347, indicating a high level of model accuracy.

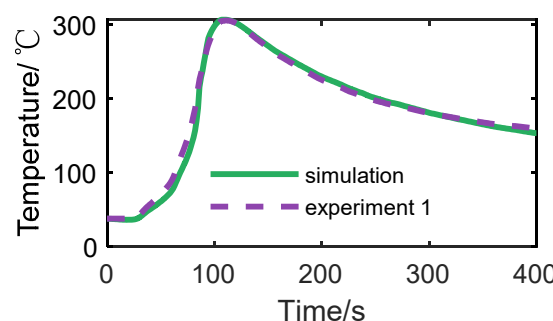


Figure 7. Comparison of sudden abuse runaway simulation and experimental temperature.

3.2. Battery Module TRP Experiments and Model Validation

Given the substantial cost and safety risks associated with conducting TRP experiments on a large scale, this section leverages the cell thermal runaway model outlined in

Section 1. The approach involves integrating the module geometry to establish a three-dimensional finite element model of the module. The geometric representation of the battery module is reasonably simplified, as depicted in Figure 8a, retaining only the battery, along with the end plates and bottom plates that maintain the battery structure.

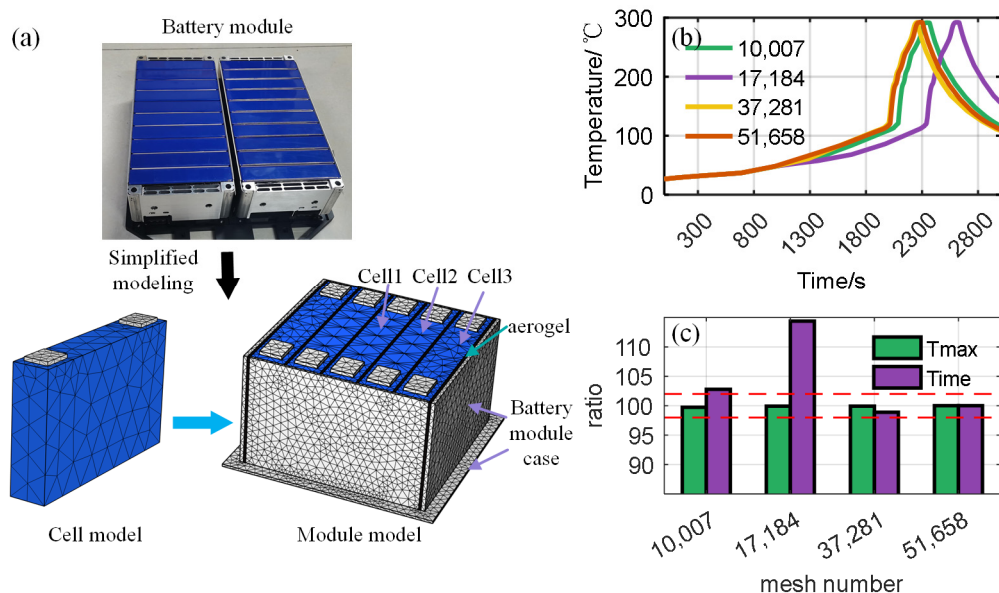


Figure 8. Numerical Model of Battery Pack. (a) Three-dimensional geometry and mesh partitioning. (b) Temperature variation in Battery 1 under overcharge thermal runaway with different numbers of meshes. (c) Comparison of the maximum temperature and corresponding time for Battery 1.

The mesh models utilized for numerical simulations involve varying numbers of meshes, specifically models with 10,007, 17,184, 37,281, and 51,658 cells. A grid independence study is conducted to ensure calculation accuracy, focusing on Battery 1's temperature, as depicted in Figure 8b, and the maximum temperature, along with the time required to reach it, as illustrated in Figure 8c. Figure 8c establishes 51,658 cells as the baseline, and the precision of maximum temperature and corresponding arrival time for the model with 37,281 cells is within 2%. Consequently, the model with 37,281 cells is selected as the reference for subsequent analyses.

Two sets of experiments were conducted to ascertain the accuracy of the TRP model. One set focused on the gradual thermal runaway resulting from fault evolution, while the other set addressed the abrupt thermal runaway induced by sudden abuse.

In consideration of further thermal protection design, aerogel protection was incorporated between the battery modules, with the initial SOC set at 100%. The specific conditions for the experimental design are detailed in Table 7.

Table 7. Scheme of experimental design for TRP.

Number	Thermal Runaway Trigger Method	Number of Trigger Cells	Protection Materials	Thickness of Protective Material	Environmental Temperature
1	Overcharge	1	Aerogel	2 mm	25~30 °C
2	Needle Puncture	2	Aerogel	2 mm	25~30 °C

(1) Battery module fault evolution thermal-runaway model validation

The left side of Figure 9 illustrates the results of the experimental model validation of TRP by triggering the thermal runaway of cell 1, providing insights into the TRP behavior of the battery module under fault evolution and model validation.

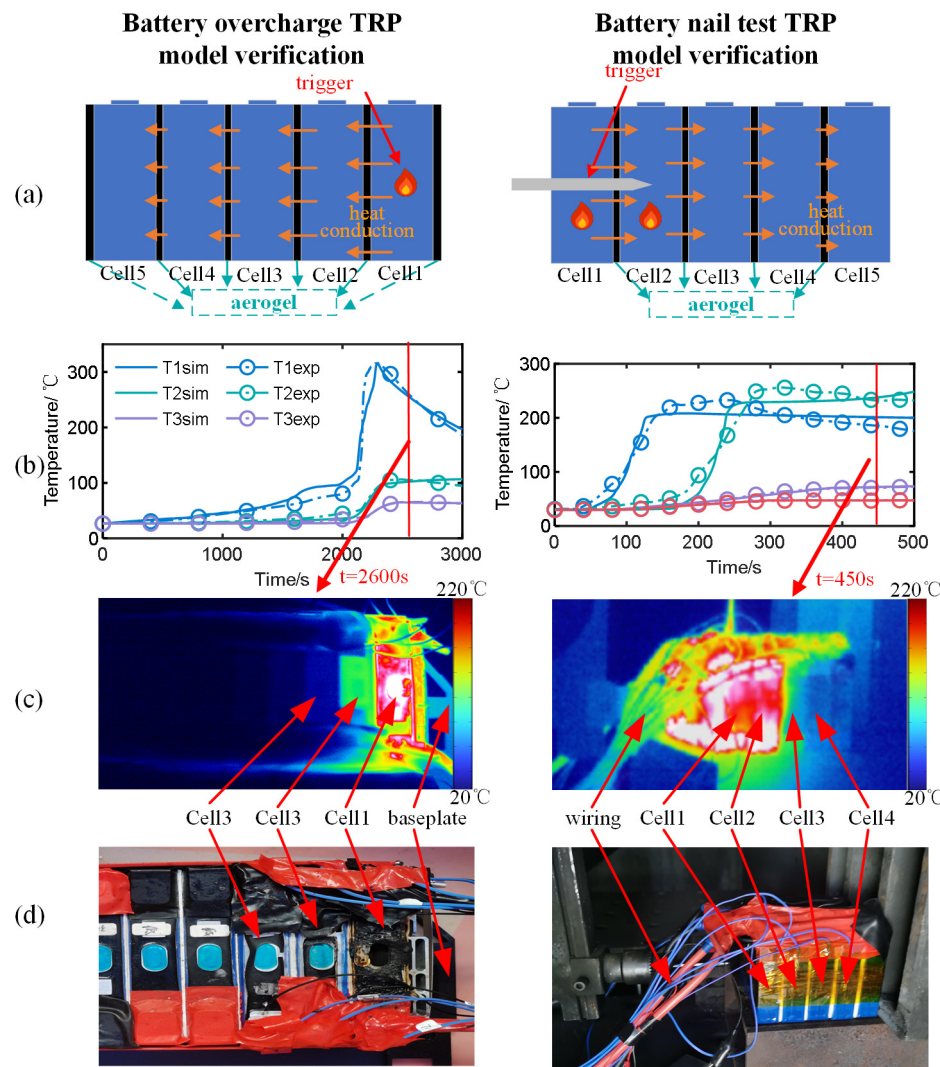


Figure 9. Battery module thermal propagation simulation experiment control diagram. **(a)** Battery TRP schematic diagram. **(b)** Battery TRP model and experimental temperature rise diagram. **(c)** Battery TRP thermal image. **(d)** Battery TRP experimental photograph.

Under an ambient temperature of 26 °C, cell 1 was overcharged at 0.5 C, reaching 129.9% SOC at 2154 s, subsequently triggering thermal runaway. The temperature of cell 1 rose to 315 °C. Due to heat propagation, the maximum temperatures of cells 2 and 3 increased to 106 °C and 65 °C, respectively, without triggering thermal runaway.

The thermal imaging on the left side of Figure 9c, captured approximately 2600 s into the experiment, reveals that, influenced by the thermal runaway of cell 1, the temperature of the battery module decreases progressively from right to left. The closer a cell is to cell 1, the more pronounced the temperature rise due to the thermal runaway influence. The left side of Figure 9d illustrates the post-experiment state of the battery module. Cell 1 experienced valve leakage and thermal runaway, while cells 2 to 4 showed no significant effects.

The battery temperature rise curves from the TRP experiment and simulation of the battery module are depicted in Figure 9b. To assess the model's accuracy, Table 8 presents the goodness of fit of the simulated temperature data. The average goodness of fit for the temperature data from cells 1 to 3 reached 0.9737, indicating a high level of model accuracy.

Table 8. Battery module temperature fitting's goodness of fit.

Goodness of Fit	Cell 1	Cell 2	Cell 3
Fault evolution	0.9824	0.98508	0.98476
Sudden abuse	0.94802	0.97524	0.99078

(2) Battery module sudden abuse thermal runaway model validation

The right side of Figure 9 illustrates the outcomes of the experimental model validation of TRP for the battery module triggered by sudden abuse. This validation induced thermal runaway in cells 1 and 2 through needle penetration.

At an ambient temperature of 29 °C, cell 1 initiated thermal runaway in 112 s, with its temperature sharply rising to 214 °C within the subsequent 50 s. Cell 2 triggered thermal runaway in 226 s, experiencing a rapid temperature increase to 250 °C in 50 s. Due to thermal propagation, the maximum temperatures of cells 3 and 4 rose to 70 °C and 47 °C, respectively, without triggering thermal runaway.

The thermal imaging map on the left side of Figure 9c captured around 450 s into the experiment reveals that cells 1 and 2 exhibit higher temperatures due to triggered thermal runaway, while cells 3 to 5 have lower temperatures. Unlike the pronounced temperature gradient observed in the fault evolution thermal runaway, the sudden abuse thermal runaway temperature cloud map can be categorized into two regions: thermal runaway and non-thermal runaway. This suggests less impact on regular batteries, resulting in a relatively low risk of thermal propagation.

The left side of Figure 9b presents the battery temperature rise curve for the TRP experiment and simulation. Table 8 outlines the goodness of fit of the simulated temperature data, with the average goodness of fit for the temperature data from cells 1 to 3 reaching 0.9713, indicating high model accuracy.

In the module overcharging experiment, a single battery triggered the thermal runaway at room temperature, and the critical battery temperature rose to 106 °C. Concerning the 141.2 °C battery venting temperature in the ARC experiment, there is a concern that when the battery pack is in a 50 °C high-temperature environment, the thermal runaway of multiple batteries may cause the thermal spread of the batteries. Therefore, further consideration is needed for the aerogel protection design. Additionally, the high precision of the established thermal spread model can effectively support the simulation analysis of thermal protection design.

4. Results and Discussion

One of the most effective safety protection strategies involves incorporating aerogel into the battery module. Utilizing the TRP model developed earlier, a safety protection design for the battery module was carried out, encompassing TRP simulations considering factors such as ambient temperature, thermal runaway triggering mode, the number of triggered thermal runaway batteries, the type of safety protection materials, and the thickness of protection materials. The TRP behavior of the battery module was analyzed under various safety protection scenarios.

4.1. Analysis of Safety Protection Strategy for TRP under Multi-Factors

A multi-factor battery module TRP simulation was conducted to analyze the impact of safety protection strategies under multiple factors. The selected influencing factors are outlined in Table 9. The maximum thickness for the protective material was set at 4 mm, resulting in a 10.75% decrease in volumetric energy density for the battery module. While this reduction in energy density is substantial, opting for a thickness beyond 4 mm is not recommended due to diminishing returns. The chosen thermal runaway triggering methods are representative of the majority of thermal runaway scenarios. The model includes five individual cells in the battery module, and triggering thermal runaway in up to 60% of the cells is sufficient to cover most scenarios. A comparative analysis

was conducted for protective materials, contrasting common aerogel protective materials with conventional insulation films used in regular modules. The material parameters are provided in Table 10. The environmental temperature was set between 20 °C and 50 °C, covering the operating temperature range of the battery module.

Table 9. Influencing factors of battery-module TRP.

Factor	Simulation Values
Thickness of protective material	0.5~4 mm
Thermal runaway trigger method	Sudden abuse/fault evolution
Thermal runaway trigger battery	1~3
Flame retardant materials	Aerogel/insulation Sheet
Environmental temperature	20 °C~50 °C

Table 10. Thermophysical parameters of protective materials.

Parameters	Insulating Sheet	Aerogel	Unit
Intensity	900	200	kg/m ³
Specific heat capacity	1900	900	J/(kg·K)
Thermal conductivity	0.24	0.022	W/(K·m)

Figure 10 depicts the TRP behavior of a multi-factor battery module with safety protection. The red points represent the occurrence of TRP, the green points represent the non-occurrence of TRP, and the red surface signifies the thermal propagation boundary of the battery module.

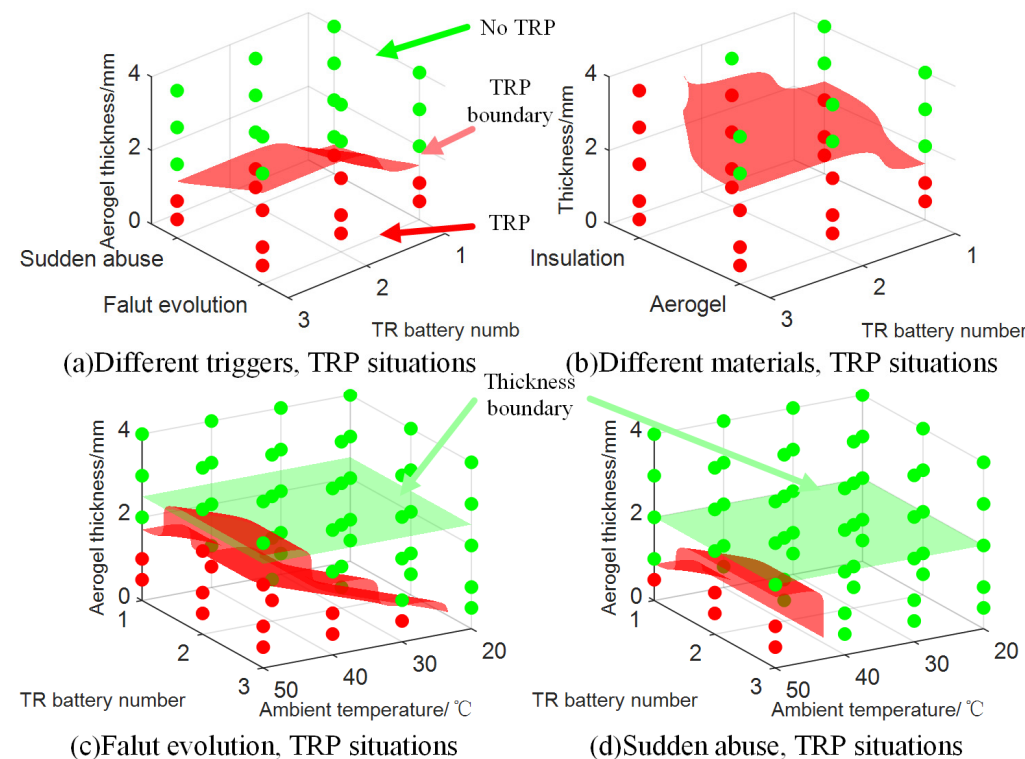


Figure 10. TRP of multi-factor battery module boundary analysis.

In Figure 10a, the impact of different thermal runaway triggering modes, the number of triggering batteries, and the aerogel thickness on the TRP behavior of the battery module are explored under high-temperature conditions (50°C). The greater the number of cells in the battery module experiencing thermal runaway, the higher the abnormal heat generated, leading to an increased risk of TRP within the battery module. Thinner aerogel thickness results in lower insulation against abnormal heat, consequently increasing the risk of TRP. Compared to rapid misuse, thermal runaway triggered by fault evolution allows for a longer duration of abnormal heat conduction between cells, posing a greater risk of thermal propagation.

Figure 10b compares the impact of aerogel safety protection material and conventional insulation film on the TRP behavior of the battery module under the condition of degradation misuse, which poses a higher risk. The comparison is conducted in a high-temperature environment of 50°C . Aerogel material, with its high thermal insulation properties, effectively reduces the risk of TRP in the battery module compared to insulation film. Additionally, as the number of cells triggering thermal runaway increases, the ability to mitigate the risk becomes more pronounced.

Figure 10c,d illustrate the impact of different environmental temperatures, the number of cells triggering thermal runaway, and the aerogel thickness on the TRP behavior of the battery module under fault evolution triggering and rapid misuse triggering, respectively. Lower environmental temperatures, fewer cells triggering thermal runaway, and thicker aerogel result in a lower TRP risk in the battery module.

Considering that an excessively thick aerogel can significantly impact the energy density of the battery module, the chosen aerogel thickness in the safety protection strategy should be as thin as possible. Therefore, for fault evolution triggering and rapid misuse triggering, the selected minimum thickness for the safety protection strategy is 2.5 mm and 1.5 mm, respectively.

4.2. Simulation Verification of Battery Module TRP Protection Strategy in the High-Temperature Environment

Based on the strategic analysis, a simulation of TRP in a battery module was conducted under typical high-temperature conditions. The simulation environment was set at 50°C , and a 2.5 mm thick aerogel safety protection strategy was chosen. Simulations were performed separately for the two thermal runaway triggering methods to assess the effectiveness of the aerogel protection strategy. The simulation results are presented in Figure 11.

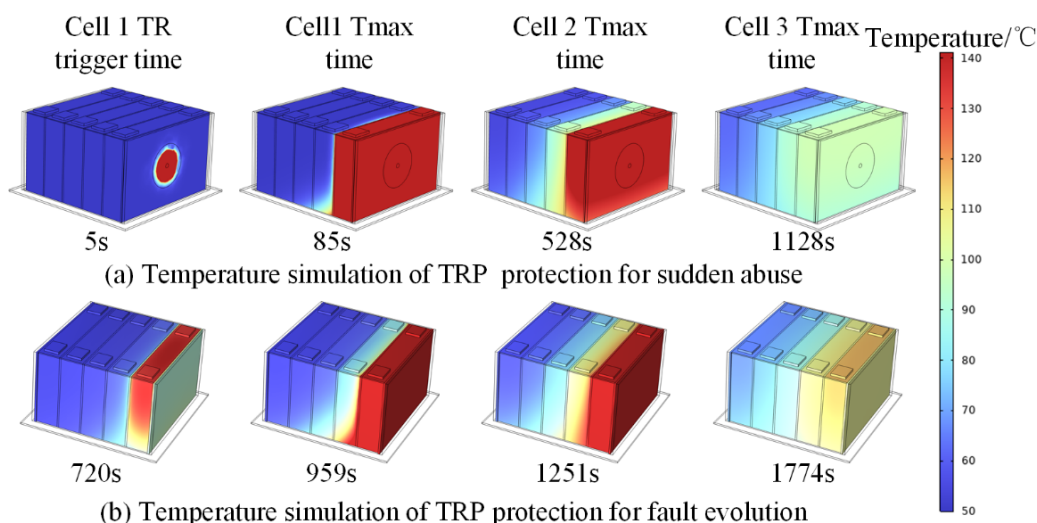


Figure 11. Simulation validation of safety protection strategy in a 50°C high-temperature environment.

Four characteristic time points were selected:

1. The moment of thermal runaway triggering of cell 1 represents the state of the battery module before TRP.
2. The moment of the highest temperature of cell 1 represents the state of the battery module triggered by thermal runaway.
3. The moment of the highest temperature of cell 2 indicates whether or not the battery module undergoes TRP.
4. The moment of the highest temperature of cell 3 represents the final state of the battery module after TRP.

The temperature distribution of the battery module was mapped with 50 °C as the lower boundary and 141.2 °C as the upper boundary. The three-dimensional temperature distribution cloud map in Figure 11 illustrates that the incorporation of aerogel protection prevents TRP within the battery module. Under both sudden abuse and fault evolution triggering, the highest temperatures of cell 2 are around 100 °C and 120 °C, respectively, below the TRP threshold. Therefore, TRP did not occur in the battery module.

With the addition of the 2.5 mm aerogel, the volumetric energy density of the battery module decreased by 5.68%, indicating a relatively minor impact. The decrease in volumetric energy density of the battery module is shown in Equation (13).

With the addition of 2.5 mm aerogel, the volumetric energy density of the battery module decreased by 5.68%, indicating a relatively minor impact. The decrease in volumetric energy density of the battery module is shown in Equation (13).

$$p = \frac{1}{1 + (d - d_0)N/d_1N_1 + d_2} \times 100\% \quad (13)$$

where d represents the thickness of the aerogel; $d_0 = 1$ mm represents the thickness of the insulating sheet between the cells in the battery module; $d_1 = 26.7$ mm represents the thickness of the battery cells; $d_2 = 16$ mm represents the sum of the thickness of the end plates on both sides of the battery module; and $N_0 = 6$ and $N_1 = 5$ represent the number of aerogel and cells, respectively.

The comprehensive analysis of the safety protection simulation for the selection of a lithium iron phosphate battery in this paper indicates that adding a 2.5 mm thickness aerogel flame-retardant protective material to the battery module effectively prevents the propagation of thermal runaway, with the volumetric energy density of the battery module decreasing by only 5.68%.

5. Conclusions

In addressing the challenge of thermal propagation in LiFePO₄ batteries, this study achieved several significant milestones and drew the following conclusions:

- (1) Comprehensive TRP model: This study successfully developed a comprehensive TRP model for battery modules. This model integrates the principles of heat generation from side reactions within batteries with the three-dimensional heat conduction equation. The establishment and calibration of a cell thermal runaway model were accomplished through ARC experiments. Two distinct thermal runaway triggering modes, namely fault evolution and sudden abuse, were identified and calibrated through relevant experiments like overcharge and needle penetration.
- (2) TRP experiments and model: Progress was made in conducting experiments and simulations on the TRP of battery packs under 1 mm aerogel safety protection, including overcharging and battery puncture scenarios. The experimental results indicate that the design with a 1 mm aerogel thickness still poses risks at room temperature, thus necessitating further analysis of thermal protection. The model validation results demonstrate high accuracy, with average goodness of fit for battery temperature being 0.98408 and 0.97134, supporting practical simulation analysis for thermal protection design.

- (3) Multi-factor analysis of safety protection design and conducting a comprehensive analysis of multi-factors in aerogel safety protection design: Based on the high-precision TRP model, a simulation analysis was carried out to evaluate the safety protection effectiveness under different aerogel safety protection strategies, considering various triggering conditions, the number of triggered batteries, and environmental temperatures. The results indicate that the safety protection design with a 2.5 mm aerogel thickness can meet the requirements of most scenarios, with only a 5.68% reduction in volumetric energy density.

In summary, this study significantly contributes to the understanding of thermal propagation challenges in LiFePO₄ batteries, offering valuable insights for enhancing battery modules' safety and reliability through aerogel-based safety protection strategies.

Author Contributions: Conceptualization, J.L.; Methodology, Z.C.; Software, Z.C., Z.L. (Ziming Liu) and Z.L. (Zhengnan Liu); Validation, Z.C. and Z.L. (Ziming Liu); Investigation, Z.L. (Zhengnan Liu); Writing—original draft, Z.C.; Writing—review & editing, J.L. and X.J. All authors have read and agreed to the published version of the manuscript.

Funding: This work was supported in part by the National Key Research and Development Program of the Ministry of Science and Technology of China under grant 2021YFB2501801, and in part by the National Natural Science Foundation of China under grant 52072037.

Data Availability Statement: The data that support the findings of this study are available on request from the corresponding author.

Acknowledgments: The authors would like to thank the National Engineering Research Center of Electric Vehicles in Beijing Institute of Technology for the support of this research project.

Conflicts of Interest: The authors declare no conflict of interest.

References

- Wen, J.; Yu, Y.; Chen, C. A Review on Lithium-Ion Batteries Safety Issues: Existing Problems and Possible Solutions. *Mater. Express* **2012**, *2*, 197–212.
- Feng, X.; Ouyang, M.; Liu, X.; Lu, L.; Xia, Y.; He, X. Thermal runaway mechanism of lithium ion battery for electric vehicles: A review. *Energy Storage Mater.* **2017**, *10*, 246–267. [[CrossRef](#)]
- Ren, D.; Liu, X.; Feng, X.; Lu, L.; Ouyang, M.; Li, J.; He, X. Model-based thermal runaway prediction of lithium-ion batteries from kinetics analysis of cell components. *Appl. Energy* **2018**, *228*, 633–644. [[CrossRef](#)]
- Bugryniec, P.J.; Davidson, J.; Brown, S. Advanced abuse modelling of Li-ion Cells—A novel description of cell pressurization and simmering reactions. *J. Power Sources* **2020**, *474*, 228396.
- Zhang, Q.W.Q. Numerical modeling on thermal runaway triggered by local overheating for lithium iron phosphate battery. *Appl. Therm. Eng. Des. Process. Equip. Econ.* **2021**, *192*, 116928.
- Feng, X.; Ren, D.; He, X.; Ouyang, M. Mitigating Thermal Runaway of Lithium-Ion Batteries. *Joule* **2020**, *4*, 743–770.
- Feng, X.; Sun, J.; Ouyang, M.; Wang, F.; He, X.; Lu, L.; Peng, H. Characterization of penetration induced thermal runaway propagation process within a large format lithium ion battery module. *J. Power Sources* **2015**, *275*, 261–273. [[CrossRef](#)]
- Feng, X.; Lu, L.; Ouyang, M.; Li, J.; He, X. A 3D thermal runaway propagation model for a large format lithium ion battery module. *Energy* **2016**, *115*, 194–208.
- GB 38031-2020; Electric Vehicles Traction Battery Safety Requirements. Standardization Administration of the People's Republic of China: Beijing, China, 2020.
- Jia, Z.; Wang, S.; Qin, P.; Li, C.; Song, L.; Cheng, Z.; Jin, K.; Sun, J.; Wang, Q. Comparative investigation of the thermal runaway and gas venting behaviors of large-format LiFePO₄ batteries caused by overcharging and overheating. *J. Energy Storage* **2023**, *61*, 106791. [[CrossRef](#)]
- Weng, J.; Ouyang, D.; Yang, X.; Chen, M.; Zhang, G.; Wang, J. Alleviation of thermal runaway propagation in thermal management modules using aerogel felt coupled with flame-retarded phase change material. *Energy Convers. Manag.* **2019**, *200*, 112071.
- Ye, Y.; Shi, Y.; Cai, N.; Lee, J.; He, X. Electro-thermal modeling and experimental validation for lithium ion battery. *J. Power Sources* **2012**, *199*, 227–238. [[CrossRef](#)]
- Spotnitz, R.; Franklin, J. Abuse behavior of high-power, lithium-ion cells. *J. Power Sources* **2003**, *113*, 81–100.
- Kong, D.P.; Ping, P.; Wang, Q.S.; Sun, J.H. Study on high temperature stability of LiNi_{0.33}Co_{0.33}Mn_{0.33}O₂/Li₄Ti₅O₁₂ Cells from the safety perspective. *J. Electrochem. Soc.* **2016**, *163*, A1697–A1704. [[CrossRef](#)]
- Kim, G.H.; Pesaran, A.; Spotnitz, R. Three-Dimensional Thermal Abuse Model for Lithium-Ion Cells. *J. Power Sources* **2007**, *170*, 476–489.

16. Ren, D.; Feng, X.; Lu, L.; Ouyang, M.; Zheng, S.; Li, J.; He, X. An electrochemical-thermal coupled overcharge-to-thermal-runaway model for lithium ion battery. *J. Power Sources* **2017**, *364*, 328–340. [[CrossRef](#)]
17. Abada, S.; Petit, M.; Lecocq, A.; Marlair, G.; Sauvant-Moynot, V.; Huet, F. Combined experimental and modeling approaches of the thermal runaway of fresh and aged lithium-ion batteries. *J. Power Sources* **2019**, *399*, 264–273. [[CrossRef](#)]

Disclaimer/Publisher’s Note: The statements, opinions and data contained in all publications are solely those of the individual author(s) and contributor(s) and not of MDPI and/or the editor(s). MDPI and/or the editor(s) disclaim responsibility for any injury to people or property resulting from any ideas, methods, instructions or products referred to in the content.